



ELSEVIER

Progress in Surface Science 74 (2003) 219–237

Progress in
SURFACE
SCIENCE

www.elsevier.com/locate/progsurf

Electron lifetimes in image-potential states at metal–dielectric interfaces

M. Machado ^{a,*}, E.V. Chulkov ^{a,b}, V.M. Silkin ^b, U. Höfer ^c,
P.M. Echenique ^{a,b}

^a *Departamento de Física de Materiales, Facultad de Química, Universidad del País Vasco (UPV/EHU)
Apdo. 1072, 20080 Donostia, Basque Country, Spain*

^b *Donostia International Physics Center (DIPC) and Centro Mixto CSIC-UPV/EHU,
Paseo Manuel de Lardizabal 4, 20018 Donostia, Basque Country, Spain*

^c *Fachbereich Physik und Zentrum für Materialwissenschaften, Philipps-Universität, Renthof 5,
D-35032 Marburg, Germany*

Abstract

We present an overview of experimental and theoretical studies of image states dynamics at metal–dielectric interfaces. The interaction of an image-state electron with a metal substrate is largely altered by the presence of a dielectric adlayer. The electron affinity of the adsorbate determines, to a great extent, the evolution of image states upon adsorption. A large variety of adsorbates and surfaces have been studied, from both experimental and theoretical points of view. On the theoretical side, penetration approaches are not able to include all the physics involved in decay processes. A more realistic many-body calculation, which takes into account all the fundamental factors determining the lifetime, has been recently performed, and a fairly good agreement with experiments has been obtained.

© 2003 Elsevier Ltd. All rights reserved.

Keywords: Image states; Dielectric adsorbates; Lifetime; Many-body calculations; Argon; Cu(100)

1. Introduction

Electronic properties at surfaces and interfaces and their dependence on the interfacial structure are of fundamental interest to various research fields. The interaction of excited surface electronic states with the underlying substrate governs the

* Corresponding author. Fax: +349-43015600.

E-mail address: wabmagam@sc.ehu.es (M. Machado).

cross-sections and branching ratios of practically all electronically induced adsorbate reactions at metal surfaces [1–4]. The dynamics of excited electrons at interfaces provides important information on electronic transport across device junctions, interaction of charges with metal–insulator interfaces, dielectrics in electronic circuits, etc. [5]. The adsorption of dielectric materials on metal surfaces modifies the energy levels, wave functions and dynamics of the excited states of a metal. In particular, it is known that adsorbates with a negative electron affinity (EA) induce a large increase in the lifetimes of image states, by decoupling the wave function from the solid substrate [6–12]. Dielectric materials, such as Xe, with positive EA give rise to quantum-well states [9,13–17]. Two-photon photoemission (2PPE) techniques have enabled this effect to be studied in a layer-by-layer way, making it possible to probe directly the nature of quantum confinement effects on electron transport.

Image states [18] are a particular class of surface states, which arise as a consequence of the interaction between an electron in the vacuum region and the polarization charge it induces in the surface. If the projected bulk-band structure of the metal has a gap close to the vacuum level, the electron can neither penetrate into the metal nor escape into the vacuum, because of the image-potential tail, whose asymptotic form is that of the classical long-range image potential:

$$V(z) = \frac{-1}{4(z - z_{\text{im}})}, \quad (1)$$

where z represents the distance from the surface and z_{im} is the image-plane position. The electron is then trapped outside the surface, forming a series of image-potential states, converging to the vacuum level. Image-state wave functions are quasi-free in the plane parallel to the surface, and are localized perpendicularly to the surface, with the maximum of the probability density located in vacuum region, beyond the metal's jellium edge.

In general, image states have longer lifetimes than surface or bulk states of the same energy, because they are mainly localized outside the crystal, which results in a small overlap with the substrate.

Experimentally, time-resolved 2PPE techniques have provided a very powerful tool to study electron dynamics both in intrinsic and image surface states [19–21]. In these experiments, a photon from a short laser pulse (pump) excites an electron from a state below the Fermi level to an intermediate empty state below the vacuum level, from which it is subsequently lifted above the vacuum level by a second photon (probe) [22]. The energy spectrum of these photo-emitted electrons may be used to determine the binding energies of the intermediate states. By varying the temporal interval between the two pulses the dynamics of the system can be monitored in real time.

In the present paper, we resume experimental and theoretical progress made in the past decade on the study of electron dynamics at metal–insulator interfaces, together with some recent advances. We will concentrate on physisorbed species, i.e., atoms or molecules that do not interact chemically with the metal surface. For the saturated monolayers (ML) and the higher adsorbate coverages that we consider in the

following, the high-energy atomic orbitals of the adlayer overlap to form a conduction band. This band can lie below or above the vacuum level and defines the EA of the adsorbate, which will be shown to play a key role in the evolution of the metal image states upon adsorption of a dielectric material. Two main cases are analyzed: negative (repulsive) EA, whose main effect is the decoupling of image states with increasing coverage and positive (attractive) EA, which leads to a quantum-well like behavior of the image states. Both experimental and theoretical descriptions of electron dynamics at various metal–dielectric interfaces, mainly alkanes and rare gases, are discussed.

The article is organized as follows: A brief overview on the main previous experimental and theoretical results on electron dynamics at metal-adsorbate systems is given in Section 2. In Section 3, we present a recently reported many-body calculation of the image-potential states binding energies and lifetimes of the Ar/Cu(1 0 0) system, as a function of coverage. These results are compared with experiments and discussed in Section 4. Finally, our conclusions are summarized in Section 5.

Unless otherwise stated, atomic units ($\hbar = m = e^2 = 1$) are used throughout.

2. Metal–dielectric interfaces: earlier work

Image-state properties on clean surfaces, which are quite well understood, suffer dramatic changes when a dielectric is adsorbed on a metal surface. Binding energies, coupling with the bulk states and lifetimes become, as we will see, significantly altered by the modified surface potential.

The time-resolved 2PPE studies that we discuss concentrate mainly on the (1 1 1) and (1 0 0) surfaces of noble metals, mostly of Cu and Ag. The electronic structures of these two crystallographic faces show important differences, which are crucial for some of the properties of image states. The overlap of the image state wave function with the surface and bulk states and its behavior in vacuum and bulk regions depend to a large extent on the position of these states with respect to the energy gap of the projected bulk band structure.

The multiple reflection theory (MRT) [23,24] predicts binding energies and the position of the maximum of the wavefunctions of image states taking into account the effect of the substrate's band structure. It considers surface states as plane waves trapped between the bulk crystal and the image potential barrier. Bound states occur when the total accumulation of the phase is $\phi_C + \phi_B = 2\pi n$, ϕ_C and ϕ_B being the phases of the crystal and the barrier reflectivity, respectively. For s–p inverted band gaps, where the bottom of the gap is p-like, while the top is s-like, ϕ_C varies from 0 to π from the bottom to the top of the gap. It is clear that, if this were the case for ϕ_B , we would have only one or no solutions, thus no surface states. However, if ϕ_B varies rapidly with energy, there are more chances of finding many solutions. States induced by a rapid variation of ϕ_C are called crystal-induced surface states, while those due to ϕ_B are barrier-induced states. The ϕ_B dependence on energy can be expressed [23], within the WKB approximation, as

$$\phi_B(E) = \pi \left[\frac{2Z_1}{\sqrt{-2E}} - 1 \right], \quad (2)$$

where

$$Z_1 = \frac{1}{4} \frac{\epsilon - 1}{\epsilon + 1}, \quad (3)$$

ϵ being the static dielectric constant of the material.

As the vacuum level is approached, the variation of ϕ_B becomes infinitely rapid, and a Rydberg series of states (image states) is created. These states are within 1 eV below the vacuum level, and in this case one can consider that ϕ_C remains constant. Taking into account the condition for the phases and Eq. (2) leads to the following expression for the binding energies of image states:

$$E_b = -\frac{0.85 \text{ eV}}{(n+a)^2}, \quad n = 1, 2, \dots, \quad (4)$$

where a , which is called the quantum defect, can be written as

$$a = \frac{1}{2} \left[1 - \frac{\phi_C}{\pi} \right]. \quad (5)$$

At the close-packed (1 1 1) surfaces, the vacuum level is close to the top of the gap, so $\phi_C \sim \pi$ and $E_b = -0.85 \text{ eV}/n^2$. For (1 0 0) surfaces, the vacuum level is at the middle of the gap and $\phi_C \sim \pi/2$, so $E_b = -0.85/(n+0.25)^2$. Therefore, with this relatively simple model it can be easily seen that image states are more tightly bound in (1 1 1) crystallographic faces than in the (1 0 0) ones. Then, it is also evident that the maximum of the probability density will be closer to the surface for the (1 1 1) case, as the states will be closer to the steep part of the Coulomb potential than at (1 0 0) surfaces.

This dependence of the overlap on the particular surface face will undoubtedly affect the image states lifetimes both at the clean surfaces and at the metal–dielectric systems.

2.1. Experimental work

The first studies of image states at metal surfaces with adsorbates were performed by means of inverse photoemission [25,26], which, unfortunately, lacks the necessary precision to an accurate determination of the binding energy shift induced by the adsorbates. 2PPE is a more suitable way to probe image-state properties in this kind on systems.

The first 2PPE experiments on metal–dielectric systems, performed by Harris and coworkers [27,28], showed that image states persist, with modified binding energies and effective masses, upon adsorption of several layers of materials, such as alkanes and rare gases. The work-function change, caused by the adsorbate, induces a shift of the vacuum level with respect to the Fermi level of the metal. As image-state binding energies remain pinned to the vacuum level, the energetic relationship of

image states with respect to the metal's band structure will be altered by the physisorption process. Lingle et al. [6,7] determined the $n = 1$ energies and lifetimes for Ag(1 1 1) with several ML of alkanes, finding that binding energies decrease when coverage increases, while lifetimes get longer. For the $n = 1$ state the lifetime shows an approximately exponential increase with growing adlayer thickness. For $n = 2$ and 3, a dramatic increase is found with adsorption of one layer, but this effect is much less pronounced for the bilayer [7].

Lingle and coworkers propose a simple picture, where the repulsive EA of the layers induces a tunneling barrier which decouples the image states from the underlying substrate. The probability density maximum of the image states is shifted away from the metal surface. In this way, coupling with electron–hole pairs in the substrate becomes less probable and lifetimes increase.

It is interesting to note that at the bare Ag(1 1 1) surface, the $n = 2$ state is shorter lived than $n = 1$ [19]. This happens because, while $n = 1$ is in the energy gap, $n = 2$ is above the top of the gap and degenerate with the projected bulk conduction band. For this kind of resonant states, the lifetime is, in general, much shorter than for states in the gap, because the overlap with bulk states is much larger. With the adsorption of an alkane monolayer, both the $n = 1$ and the 2 state get decoupled from the metal, the work-function change lowers the $n = 2$ state into the gap and its lifetime becomes longer (270 fs) than that of $n = 1$ (155 fs) [7].

Dielectric materials with attractive EA add interesting effects to the physics of image states outside insulator layers. McNeill et al. [13] reported measurements of energies and dispersions of image states for several ML of Xe on Ag(1 1 1). They found that, while the $n = 1$ state evolves as an image state screened by the dielectric layers, i.e., its probability density shifts toward the vacuum region with increasing coverage, the $n = 2$ and 3 states become quantum-well electronic states of the layer. The second and third image states evolve from their purely two-dimensional free-like behaviour (image states are only bound in the direction perpendicular to the surface) to the three-dimensional conduction bulk bands of Xe. The main reason for this is the attractive electron affinity, which gives rise to a quantum well potential bounded by the band gap of the metal substrate and the image potential. This quantum well confines the image state electron within the layer at high coverage.

This confinement effect was also found to influence the lifetimes of the first three image states of 1–6 ML of Xe on Ag(1 1 1) [14]. While the $n = 1$ lifetime increases with the number of layers, the $n = 2$ and 3 lifetimes oscillate with increasing coverage as the layer boundary crosses the wave-function nodes.

The same trend was reported for Xe/Cu(1 1 1) in [9] whereas the strongly repulsive N₂ layers on the same substrate showed a drastic decrease of binding energies and increase of lifetimes, similar to the alkane layers on Ag(1 1 1). In an earlier publication, Wolf et al. [29] had already reported the binding energies and lifetimes of the $n = 1$ and 2 image states for one monolayer of Xe/Cu(1 1 1). They pointed out the importance of the decreased work-function upon Xe adsorption on the bulk penetration of the image-state wavefunctions. At the bare Cu(1 1 1) surface (see Fig. 1), the $n = 1$ state is located near the top of the projected band gap, while $n = 2$ lies above the gap and strongly couples with bulk states. The monolayer lowers the

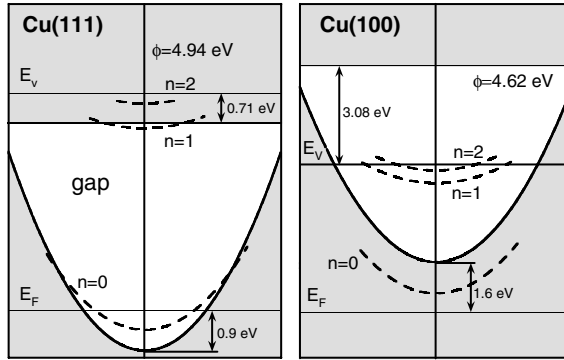


Fig. 1. Surface projected band structure of Cu(111) and Cu(100) surfaces. Shaded areas represent regions outside band gap, where bulk states exist. While in Cu(100) whole image state series is within band gap, in Cu(111) only the $n = 1$ state lies in gap.

energy of the $n = 1$ state, shifting it toward the center of the gap, where its wave function is more decoupled from the bulk substrate. As a consequence, the lifetime increases from 18 to 75 fs and its binding energy decreases (smaller quantum defect). However, for $n = 2$, the workfunction change of -0.5 eV is not sufficient to remove its degeneracy with the bulk states. It remains slightly above the top of the gap. Nevertheless, its lifetime increases from 17 to 40 fs, suggesting that the Xe layer shifts its probability density toward the vacuum region [9,29].

A systematic study that compares the effect of Ar, Kr, and Xe rare-gas layers on the properties of image states on Cu(100) has recently been conducted by Berthold et al. [30]. The original 2PPE data for Ar/Cu(100) of Fig. 2 demonstrate the high

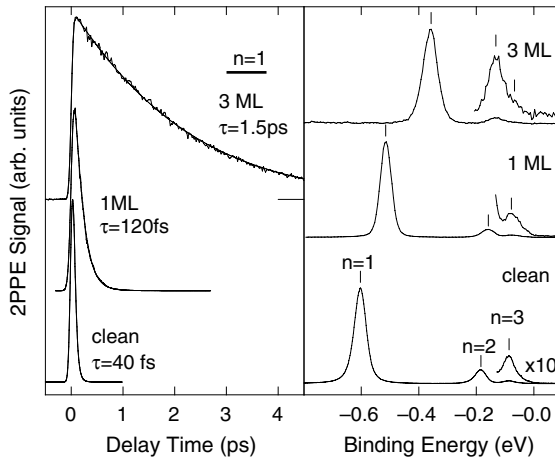


Fig. 2. 2PPE spectra (right) and pump-probe curves (left) for clean Cu(100) and for 1 and 3 ML of Ar (adapted from [12]).

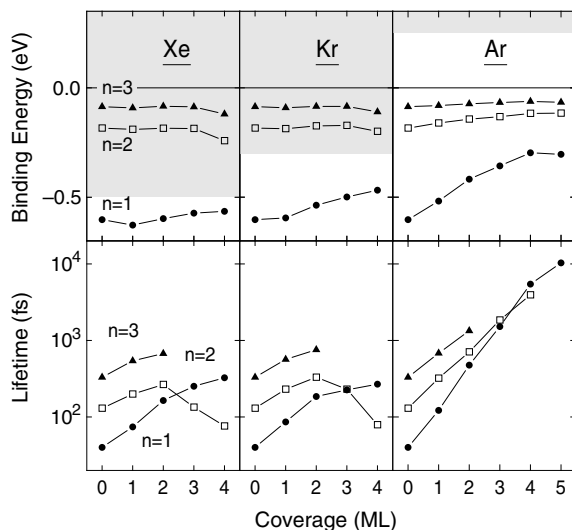


Fig. 3. Experimental energies (top) and lifetimes (bottom) obtained for the rare gases xenon, krypton and argon adsorbed on Cu(100) as function of monolayer coverage. Shaded areas indicate the conduction bands of the adlayers (adopted from [30]).

accuracy of these measurements. Binding energies and lifetimes determined for the states $n = 1, 2, 3$ plotted as function of layer thickness for the three adsorbates are collected in Fig. 3. The comparison directly shows the qualitatively different behavior of adsorbates with positive EA (Xe, Kr) and negative EA (Ar). Argon layers (EA = +0.25 eV) are repulsive for all image states, the lifetimes increase nearly exponentially with layer thickness, while the binding energies decrease monotonously. This is fully consistent with the Ar layers presenting a tunnelling barrier for the image-state electron. With increasing layer thickness the image attraction of the metal as well as the interaction with the metal surface is reduced. The result is a reduced binding energy and a considerably prolonged lifetime. The effect of the Ar adlayers is less dramatic for $n = 2$ and 3 state than for $n = 1$ because the energy of these higher lying states is closer to the top of the Ar conduction band. For this reason the height of the tunnelling barrier is smaller, and the lifetime of the $n = 2$ state, e.g., can even get shorter than that of $n = 1$ [30].

The influence of Kr (EA = -0.3 eV) and Xe layers (EA = -0.5 eV) on the $n = 1$ state is similar but weaker than that of Ar layers because, again, the height of the tunnelling barrier is smaller. This effect overcompensates the somewhat increased layer thickness of these rare gases at the same coverage. The higher quantum states $n \geq 2$ are degenerate with the Xe or Kr conduction band. They can penetrate the layers and the lifetimes of the image-states exhibit the quantum-well-like oscillations of the lifetimes as function of coverage as described above for Xe/Ag(111).

In the results of Berthold et al. [11,30] the main effects of dielectric adsorbates on the properties of image states are revealed in a rather clear way. At the noble metals

(100) surfaces (Fig. 1) the vacuum level and the Rydberg series are located near the center of the band gap. For this reason, the work function shift in the adsorption process does not induce, as was the case for (111) surfaces, a significant change in the position of the image states within the gap. They stay close to its center in all cases. In addition the electronic structure of the light rare-gases like argon is relatively simple and well known. This makes these experimental results particularly interesting for comparison with theory.

2.2. Theoretical models

The most often used approximation for studying the modification of the surface potential of a metal, due to adsorption of dielectric overlayers is the dielectric continuum model (DCM), first proposed by Cole [31,32] and modified by Harris and coworkers [13,17]. Within this approach, the adsorbed dielectric layers are treated as a homogeneous, structureless continuum characterized by its dielectric constant, the effective mass of the conduction band and the EA. In particular, the EA of the adsorbate plays an important role in the DCM. It increases or decreases the electrostatic potential within the dielectric layers, taking into account that the dielectric has a band structure.

In the DCM, the electron in the image state is considered quasi-free in the plane parallel to the surface, and bound in the perpendicular direction by a one-dimensional model potential. This potential is calculated inside the layer and vacuum regions from classical electrostatics, and can be expressed as [7,10,15,17]

$$\begin{aligned}
 V(z) &= EA - \frac{1}{4\epsilon z}, \quad 0 < z < t, \\
 V(z) &= \frac{-\beta}{4(z-t)} + \frac{1-\beta^2}{4\beta} \sum_{k=1}^{\infty} \frac{(-\beta)^k}{z-t+kt}, \quad z > t,
 \end{aligned}
 \tag{6}$$

where $\beta = (\epsilon - 1)/(\epsilon + 1)$, t is the width of the dielectric and z is the distance, referred to the metal's jellium edge, in the direction perpendicular to the surface. The divergence at $z = t$, i.e., at the dielectric–vacuum interface, is avoided by imposing a constant potential in the range $t < z \leq t + b$, where b is a cutoff parameter. At the metal–dielectric interface, the divergence is removed by choosing a cutoff energy, usually the Fermi energy of the metal. This potential is illustrated schematically in Fig. 4 for the case of a repulsive EA material.

Inside the dielectric region, the potential of (6) describes the interaction between the excess electron and the adlayer by means of the bulk EA (first term), modified by the (screened) image potential of the metal (second term). The first term in the vacuum region corresponds to the image potential of an excess electron outside an infinite dielectric. The second term is a sum over infinite image charges inducing successive image charges as a consequence of the presence of more than one interface. Variations of this potential have been used by some authors [7,14] to treat metal–dielectric systems.

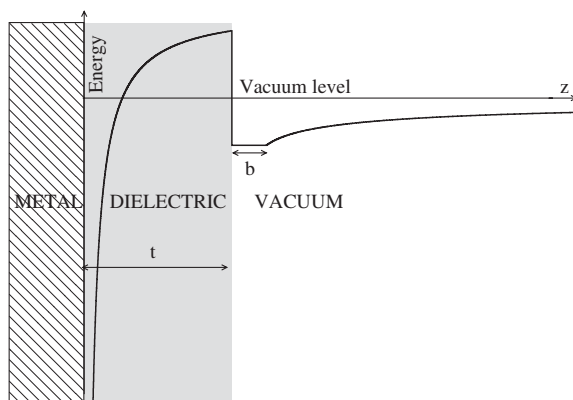


Fig. 4. Example of dielectric continuum model potential (solid line), in arbitrary units, for a negative EA dielectric of thickness t adsorbed on a metal surface. Potential is modified over a range b in order to avoid divergences.

The effect of the dielectric on the image states binding energies can be analyzed from (6). The dielectric screens the image potential of the metal (second term of both equations), but on the other side, the excess electron polarizes the adlayer, adding an attractive interaction, which appears in the first term of the potential in the vacuum region. For the monolayer case, binding energies of image states are the result of these two competing effects. As we have seen, as the number of adsorbed layers increases, the EA of the dielectric exerts also an important influence on the image-states character and dynamics.

Binding energies and wave functions are obtained straightforwardly from the DCM, by solving the Schrödinger equation. In general, the DCM has been proved to reproduce quite well the experimental trends for binding energies [9,13,14,16]. Lifetimes, however, are not included in this description and further approximations are needed.

The first self-energy calculations of the inverse lifetime broadening of image states on noble metal surfaces, were reported in [33]. In this calculation, hydrogenic-like states were used, with no penetration into the solid, to describe the image-state wave functions, a step model potential was introduced to compute the bulk final-state wave functions, and a simplified free-electron gas model was used to approximate the screened Coulomb interaction. More realistic wave functions, allowing for penetration of the electron into the crystal, were introduced in [34]. The approximations used in [33,34] for bulk and image states, as well as for the surface screening allowed qualitatively correct results for the lifetimes on the (1 1 1) and (1 0 0) surfaces to be obtained. Later, Gao and Lundqvist [35,36] proposed an even simpler model for the decay of the $n = 1$ image state on the (1 1 1) surfaces. They used an unscreened Coulomb potential, simulated the final bulk states by a single band and, in addition, included in the model the surface state as a decay channel.

Other authors have estimated the lifetime of an image state by assuming that it is inversely proportional to the part of the probability density, which overlaps with the metal substrate [43], i.e., the penetration of the image state into the bulk, viz.,

$$p_n = \int_{-\infty}^0 \psi_n^* \psi_n dz. \quad (7)$$

The linewidth of the image state with energy E_n is determined from the linewidth of a bulk state with the same energy, $\Gamma_b(E_n)$, scaled by the penetration of the image state:

$$\Gamma(E_n) = p_n \Gamma_b(E_n). \quad (8)$$

The value of $\Gamma_b(E_n)$ can be obtained either from first-principles calculations or from the experiment.

Image-state lifetimes for the Xe/Cu(1 1 1) system have been obtained [9] via this penetration approach. Experimental trends were reproduced for $n = 1$ lifetimes as a function of coverage. Decay rates for Xe/Ag(1 1 1) were calculated by McNeill et al. [14] using photoemission data for $\Gamma_b(E_n)$. They obtained qualitative agreement with experimental data and were able to reproduce the oscillations in the lifetime of $n = 2$ and 3 states, due to their quantum-well character. In the case of Ar/Cu(100), Berthold et al. [11], showed that the continuum model plus a lifetime calculation based on penetration arguments, failed to describe satisfactorily the lifetime dependence on coverage. The $n = 1$ lifetime was overestimated by factors of 3, 5 and 10 for 3, 4 and 5 ML, respectively.

Recently, a more accurate study of the influence of adsorbates on image-state properties has been performed by Marinica et al. [12] on Ar/Cu(1 0 0) systems. The interaction between the excess electron and the Ar/Cu(1 0 0) system was modeled by a two-term potential. The first one includes the electron–Cu interactions and was taken from the work of Chulkov et al. [37,38]. The second term contains the sum of the individual electron–Ar interactions, including a short-range part as well as a long-range part, due to mutual polarization effects between Ar atoms. Wave functions were obtained by solving the Schrödinger equation using a 3D wave packet propagation method [44,45]. Lifetimes of image states were approximated from the expression

$$\tau_{n,\text{Ar/Cu}(100)} = \frac{\tau_{n,\text{Cu}(100)} \cdot p_{n,\text{Cu}(100)}}{p_{n,\text{Ar/Cu}(100)}}. \quad (9)$$

By using the experimental lifetime of the clean metal image states in (9), Marinica et al. included some of the physics involved in the decay rate of the metal image states. The effect of the adsorbate was taken into account in the calculation of the wave functions. For the determination of the lifetime of the metal–dielectric image states only effects due to the ratio between the new penetration value upon adsorption and its value at the clean metal were considered. This constitutes quite a successful and computationally simple approach, and results obtained show good agreement with experimental data.

However, from time-resolved 2PPE measurements we know that the linewidth of the $n = 1$ state on Cu(111) and Cu(100) is 30 and 16.5 meV, respectively, while accurate model potential calculations [38] give penetrations of 0.22 and 0.05. Therefore, line widths differ by a factor of 2 and penetrations by a factor of 4. This example shows that the simple application of (8) or (9) can not, in general, give a realistic description of the decay rates of image states. Contributions of the evanescent tails of bulk states outside the crystal [39] and of the intrinsic surface states, together with the dynamically screened Coulomb interaction [46,47], have to be considered as well. All these key ingredients are included in the many-body calculation of image-state binding energies and lifetimes that we present in the following sections, for the case of 0–4 monolayers of Ar/Cu(100).

3. Many-body calculation of image-potential state lifetimes

Inelastic scattering rates of image states at the Ar/Cu(100) system have been obtained by Machado et al. [48] by means of a many-body calculation, based on the electronic self-energy. Within this approach, the inelastic linewidth (or inverse lifetime) of an electron in the initial state $\phi_i(\mathbf{r})$ with energy E_i is given by the projection of the imaginary part of the electron self-energy, Σ , onto this initial state [49]:

$$\tau^{-1} = -2 \int d\mathbf{r} \int d\mathbf{r}' \phi_i^*(\mathbf{r}) \text{Im}\Sigma(\mathbf{r}, \mathbf{r}'; E_i) \phi_i(\mathbf{r}'). \quad (10)$$

The self-energy is computed in the GW approximation [50], which represents the first term in a series of Σ , in terms of the Coulomb screened interaction, $W(\mathbf{r}, \mathbf{r}'; \omega)$. The evaluation of the exact many-body Green function of the system is extremely complicated and, in general, one has to resort to perturbation theory. Usually, it is the non-interacting Green function, G^0 , which is used in practice. This is known as the G^0W^0 approximation, where W^0 indicates that the screened interaction is obtained at the RPA level. Self-consistent GW calculations are not systematically better than G^0W^0 , and it is not trivial to find a way to go beyond this approximation satisfactorily [51,52].

The screened Coulomb interaction, $W(\mathbf{r}, \mathbf{r}'; \omega)$ is related to the creation of electron–hole pairs in the metal, which is the main process through which image states decay into the solid:

$$W(\mathbf{r}, \mathbf{r}'; \omega) = v(\mathbf{r}, \mathbf{r}') + \int d\mathbf{r}_1 \int d\mathbf{r}_2 v(\mathbf{r}, \mathbf{r}_1) \chi(\mathbf{r}_1, \mathbf{r}_2; \omega) v(\mathbf{r}_2, \mathbf{r}'), \quad (11)$$

where $v(\mathbf{r}, \mathbf{r}')$ and $\chi(\mathbf{r}_1, \mathbf{r}_2; \omega)$ are the bare Coulomb interaction and the response function of the interacting electron system, respectively. The response function is obtained within the random phase approximation (RPA) [49,53], by solving an integral equation for the induced potential in real space:

$$\chi^{\text{RPA}}(\mathbf{r}, \mathbf{r}'; \omega) = \chi^0(\mathbf{r}, \mathbf{r}'; \omega) + \int d\mathbf{r}_1 \int d\mathbf{r}_2 \chi^0(\mathbf{r}, \mathbf{r}_1; \omega) \frac{1}{|\mathbf{r}_1 - \mathbf{r}_2|} \chi^{\text{RPA}}(\mathbf{r}_2, \mathbf{r}'; \omega), \quad (12)$$

where $\chi^0(\mathbf{r}, \mathbf{r}'; \omega)$ is the density-response function of noninteracting electrons [54].

The inverse lifetime can be expressed as the sum over all the possible final states of the projection over the initial and final states of the imaginary part of the screened Coulomb interaction:

$$\tau^{-1} = 2 \sum_f \int d\mathbf{r} \int d\mathbf{r}' \phi_i^*(\mathbf{r}) \phi_f^*(\mathbf{r}') \text{Im}[-W(\mathbf{r}, \mathbf{r}'; E_i - E_f)] \phi_i(\mathbf{r}') \phi_f(\mathbf{r}). \quad (13)$$

Assuming that the charge density and the one-electron potential are constant in the (x, y) plane parallel to the surface, so that all variations occur in the z -direction perpendicular to the surface, wave functions of the following form can be taken:

$$\phi_n(\mathbf{r}) = \frac{e^{i\mathbf{k}_{\parallel} \cdot \mathbf{r}_{\parallel}}}{\sqrt{A}} \psi_n(z), \quad (14)$$

where A is the normalization area of the surface and \mathbf{k}_{\parallel} is the momentum parallel to the surface. The resulting expression for the scattering rate is then

$$\tau^{-1} = 2 \sum_f \int \frac{d\mathbf{q}_{\parallel}}{(2\pi)^2} \int dz \int dz' \psi_i^*(z) \psi_f^*(z') \text{Im}[-W(z, z'; \mathbf{q}_{\parallel}; E_i - E_f)] \psi_i(z') \psi_f(z), \quad (15)$$

$W(z, z'; \mathbf{q}_{\parallel}; E_i - E_f)$ being the two-dimensional Fourier transform of the screened Coulomb interaction.

The computation of the full response function of the metal–dielectric system is a very demanding task. The whole system cannot be described properly by means of a one-dimensional model, which would not account for the free-electron-like behaviour of the electrons in the metal, together with the confinement of the electrons in the Ar layer. In [48], the screened interaction of the whole system was replaced by that of the clean metal substrate, obtained from the one-dimensional model potential described in [37,38].

This potential is averaged in the plane parallel to the surface and varies in the z direction, perpendicular to the surface plane, approaching the classical image-potential tail in the vacuum region. The width and position of the energy gap at the \bar{T} point, as well as the experimental binding energies of the surface and first image state, are exactly reproduced within this model. Moreover, the potential has been proved to accurately predict the broadening of surface and image states on metal surfaces [37–42].

A modification of this approach which takes into account the effect of the adsorbate on the evanescent tails of bulk states with the same approximations as for clean metal surfaces is currently in progress [55].

The main effect of the adsorbate layers is to change the surface potential and, therefore, the image-state wave function. The effect of the dielectric films consisting

of discrete atomic layers was included in [48] by extending the DCM by an atomic potential [30]. In the former the electronic structure was accounted for by the electron affinity (EA) as a constant potential offset, which is now replaced by

$$V_{\text{atom}}(z) = V_0 - \sum_{i=1}^{n_{rg}} V_{\text{core}} \exp(-|z - d_{rg} \times (i + 1/2)|/l_{scr}), \quad (16)$$

$d_{rg} = 3.04 \text{ \AA}$ being the Ar interlayer spacing and n_{rg} the number of Ar layers. This potential generates a delocalized conduction band and a localized valence band and core level for a bulk crystal. The parameters $V_0 = -1.06 \text{ eV}$, $V_{\text{core}} = 538.8 \text{ eV}$ and $l_{scr} = 0.05 \times d_{rg}$ are adjusted in order to give the correct values for the bulk Ar electron affinity and effective mass, $EA = +0.25 \text{ eV}$ [56] and $m_{\text{eff}} = 0.47$ [57], respectively. The divergences of this classical potential are removed by restricting it to the minimum of the metal potential at the metal/rare gas interface and by interpolation across the rare gas/vacuum region for a distance of $0.3 \times d_{rg}$. The dielectric constant ($\epsilon = 1.70$ for Ar) is fixed at $\epsilon_{\text{calc}} = 1 + 0.5(\epsilon - 1) = 1.35$, in order to reproduce the experimentally observed binding energies of the image-potential states.

The dielectric properties of the metal plus adsorbate system are still described by the DCM in this model. One should note, however, that the dielectric character of the adsorbate is taken into account for the evaluation of image state wave functions, while the screened Coulomb interaction entering the linewidth evaluation is just the clean metal one.

The resulting model potential is plotted in Fig. 5 for the case of 2 ML of Ar on Cu(100) (solid line), together with the probability density of the first image state (dotted line). For comparison, the potential and the probability density of clean Cu(100) (thin solid and thin dotted lines, respectively) have been included. The

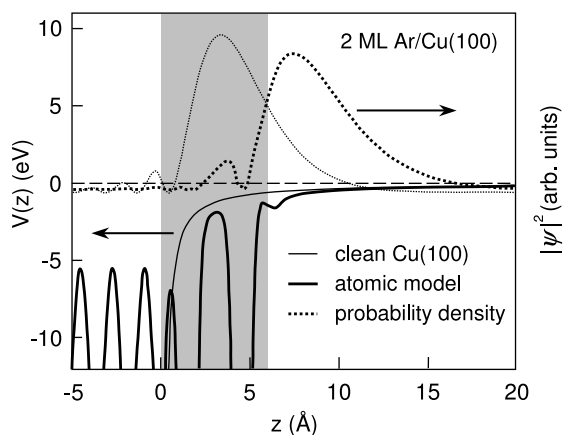


Fig. 5. Example of model potential (thick solid line) and calculated $n = 1$ probability density (thick dotted line) for 2 ML of Ar. For comparison potential and probability density of clean Cu(100) are also shown (thin lines). Shaded region indicates the adlayer, the metal jellium edge is at $z = 0$.

jellium edge (half an interlayer distance beyond the last atomic plane) is placed at $z = 0$. The shaded region indicates the position of the adlayer.

The introduction of a corrugation of the potential accomplished by Eq. (16) has two main effects on the wavefunctions of the image-potential states that influence their binding energies and lifetimes. The fast oscillations in the Ar layer effectively reduce the amplitude close to the metal surface and prevent that the smooth $-\frac{1}{4ez}$ part of the $V(z)$ of the continuum model drags to a large fraction of the wavefunction towards the metal surface. This results in smaller binding energies and longer lifetimes as obtained from a continuum model with similar parameters. If one disregards the atomic oscillations of the wavefunction, the corrugation has still the effect of reducing the effective mass m_{eff} of the electron in the Ar layer. This reduced mass spreads the wavefunction by factor $1/m_{\text{eff}}$ in z -direction. This second effect is very important for thicker layers and results in a description of the quantum-well features (in particular the relative minima and maxima of the lifetimes as function of layer thickness) that agree quantitatively with the experiment [30].

4. Results and discussion

Clean Cu(1 0 0) has a work function of 4.62 eV and the vacuum level is close to the middle of the gap, together with the Rydberg series of image states (see Fig. 1). Adsorption of 1 ML of Ar shifts the work function to 4.38 eV and the first image state is 88 meV closer to the new vacuum level.

In Fig. 6 we have plotted schematically the energy levels at the central region of the projected band gap for Cu(1 0 0) and 1 ML of Ar/Cu(1 0 0). Both the $n = 1$ and 2 states become less bound with increasing coverage, as in Fig. 7, where we have plotted our calculated energies (with respect to the vacuum level) for the first and second image state as a function of coverage, together with the time-resolved 2PPE experimental results. The $n = 1$ state experimental energy decreases from -0.602 eV

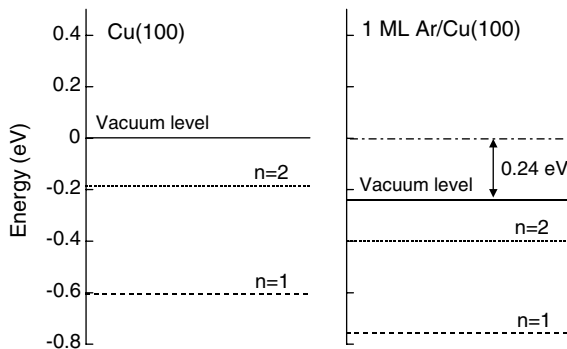


Fig. 6. Vacuum level and image states energy shift upon adsorption of 1 ML Ar on Cu(1 0 0). Energies are given in eV. Work function is reduced by 0.24 eV with Ar adsorption. Image states, which are pinned to vacuum level, become less bound in the Ar/Cu(1 0 0) system.

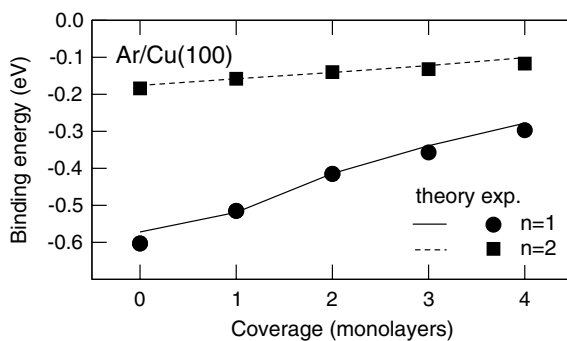


Fig. 7. Calculated and experimental energies of $n = 1$ and 2 states for 0–4 ML Ar coverages. Solid line and circles stand for theoretical and experimental results for $n = 1$. Dashed line and squares show theoretical and experimental results for $n = 2$.

at the clean surface up to -0.297 eV for 4 ML. The second image-state energy shows a weaker dependence on Ar coverage.

Fig. 8 displays the calculated probability density of $n = 1$ and 2 states, from 0 to 4 ML of Ar/Cu(100). Dotted vertical lines indicate the end of the adlayer region. The probability density maximum is displaced toward the vacuum region as the adlayer coverage increases. With 4 ML, the $n = 1$ probability density maximum is almost 28 atomic units away from the metal jellium edge, around 20 a.u. more than for the clean surface one. The penetration of the $n = 1$ wave function into the metal substrate reduces from 5.2% at Cu(100), to 1.24% for 1 ML and 0.036% for 4 ML. This strong decoupling effect is mainly a consequence of the negative EA of the Ar layers. It can be easily seen that the binding energy shift does not displace the image states series much from the gap center. Therefore, the penetration of the wave functions

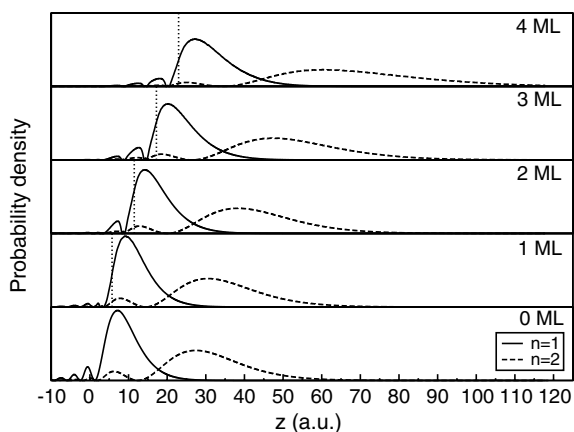


Fig. 8. Calculated probability density for $n = 1$ (solid line) and $n = 2$ (dashed line), for 0–4 ML Ar/Cu(100). Position of last Ar plane is shown with dotted line. $z = 0$ corresponds to metal jellium edge.

into the bulk will not be affected by the change in the relative position of image states with respect to band edges, as was the case for (111) surfaces. The bottom of the conduction band in Ar lies above the vacuum level (0.25 eV in bulk Ar), so that the layers act on the image states as a repulsive potential barrier. Growing layer thickness pushes the image-state wave functions farther into the vacuum region, reducing the coupling with the bulk states.

The decay rates of image states at metal–dielectric surfaces have been estimated in the literature, as we have seen, mostly from the overlap of the image-state wave function with the substrate. This coupling, weighted by the screened interaction, is responsible for the decay of image states due to electron–hole pairs creation. In our model potential calculations, penetration into the bulk for the clean Cu(100) $n = 1$ state is about 4.5 larger than for the $n = 1$ state of the 1 ML Ar/Cu(100), while the experimental lifetime of $n = 1$ in 1 ML Ar/Cu(100) is only three times the $n = 1$ lifetime at the clean surface. Therefore, although it is clear that the reduction of penetration of image states in the presence of noble gas adlayers is essential for the increase of the lifetimes, this effect cannot explain by itself all the influence of the adlayer on the image-state dynamics, and all the physics involved in lifetime calculations. A deeper understanding of the decay rates must be obtained from a more detailed study of the main factors involved in our description of decay processes. In our approach, both the coupling between initial and final states and the imaginary part of the Coulomb screened interaction are included in the evaluation of the lifetimes. The Coulomb interaction, $\text{Im}(-W(z, z', \mathbf{q}_{\parallel}; \omega))$, incorporates the effects of screening in the metal, enhancing the probability of decay processes by electron-hole pair creation at the surface region. The contribution of each state lying in energy below the image state of interest is also considered. The line width of each image state will include in this way the contribution of the intrinsic surface states, if present, and of the lower-lying image states.

Fig. 9 shows the results for the lifetimes of the first and second image state of the Ar/Cu(100) system, from 0 to 4 ML, together with the corresponding experimental

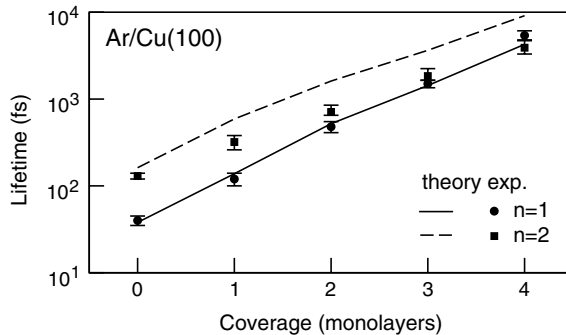


Fig. 9. Calculated and experimental lifetimes (fs) of $n = 1$ and 2 states for 0–4 ML Ar coverages. Solid line and circles stand for theoretical and experimental results for $n = 1$, respectively. Dashed line and squares show theoretical and experimental results for $n = 2$.

results. Both for $n = 1$ and $n = 2$ one can see a large increase in the lifetime of the systems with 1 or more monolayers with respect to the clean surface values. Note that lifetimes are plotted in logarithmic scale, showing clearly the exponential raising of lifetimes with increasing coverage. For the $n = 1$ state, we find very good agreement between theory and experiment for 0–4 MLs. For the second image state, theoretical results for lifetimes are systematically longer than the experimental ones.

The contribution of the lower-lying image states contains a substantial amount of the $n = 2$ and higher states linewidth. In our case, the first image state contributes as much as 28% to the total decay rate of the second image state for 1–4 ML of Ar/Cu(100).

A detailed analysis of the contribution of bulk, vacuum and interference regions to the line width of image states can be found in [48]. The partial compensation between the vacuum and interference terms explains the good results obtained by penetration models for the Ar/Cu(100) system. The error made by neglecting the vacuum and interference contributions (i.e., by considering only penetration into the bulk) is small for the clean surface, but increases with Ar coverage.

5. Conclusions

We have reviewed the experimental and theoretical work on image-potential states evolution at metal–dielectric interfaces. In general, the binding energies and the lifetimes of image state electrons are strongly modified by the presence of dielectric overlayers. The EA of the adsorbate largely determines the evolution of image states upon adsorption. Adsorbates with repulsive EA decouple the image states from the metal substrate. An attractive EA can give rise to a quantum-well behaviour of the image states at high coverage.

We have described the experimental results on a variety of surfaces and adsorbates, together with the first theoretical attempts to evaluate binding energies and lifetimes. We have discussed a recent many-body calculation of lifetimes for several argon layers on Cu(100). This approach is based on the calculation of the electronic self-energy and takes into account the different factors that determine decay processes: the coupling between initial and final states, the available decay channels and the imaginary part of the screened Coulomb interaction. The results obtained are in good agreement with experiments, especially for the first image state.

Acknowledgements

Support from the Basque Departamento de Educación, Universidades e Investigación, the University of the Basque Country UPV/EHU (9/UPV 00206.215-13639/2001), the Spanish Ministerio de Ciencia y Tecnología (MAT2001-0946), and the Max Planck Research Award funds is gratefully acknowledged.

References

- [1] E.W. Plummer, *Science* 277 (1997) 1447.
- [2] M. Wolf, G. Ertl, *Science* 288 (2000) 1352.
- [3] P. Feulner, D. Menzel, in: H.L. Dai, W. Ho (Eds.), *Laser Spectroscopy and Photochemistry on Metal Surfaces*, World Scientific, Singapore, 1995, p. 627; W. Wurth, D. Menzel, *Chem. Phys.* 251 (2000) 141.
- [4] H. Petek, M.J. Weida, H. Nagano, S. Ogawa, *Science* 288 (2000) 1402.
- [5] X.-Y. Zhu, *Ann. Rev. Phys. Chem.* 53 (2002) 221.
- [6] R.L. Lingle, Jr., D.F. Padowitz, R.E. Jordan, J.D. McNeill, C.B. Harris, *Phys. Rev. Lett.* 72 (1996) 2243.
- [7] R.L. Lingle, Jr., N.-H. Ge, R.E. Jordan, J.D. McNeill, C.B. Harris, *Chem. Phys.* 205 (1996) 191.
- [8] N.-H. Ge, C.M. Wong, R.L. Lingle, Jr., J.D. McNeill, K.J. Gaffney, C.B. Harris, *Science* 279 (1998) 202.
- [9] A. Hotzel, G. Moos, K. Ishioka, M. Wolf, G. Ertl, *Appl. Phys. B* 68 (1999) 615.
- [10] A. Hotzel, M. Wolf, J.P. Gauyacq, *J. Phys. Chem. B* 104 (2000) 8438.
- [11] W. Berthold, P. Feulner, U. Höfer, *Chem. Phys. Lett.* 358 (2002) 502.
- [12] D.C. Marinica, C. Ramseyer, A.G. Borisov, D. Teillet-Billy, J.P. Gauyacq, W. Berthold, P. Feulner, U. Höfer, *Phys. Rev. Lett.* 89 (2002) 046802.
- [13] J.D. McNeill, R.L. Lingle, Jr., R.E. Jordan, D.F. Padowitz, C.B. Harris, *J. Chem. Phys.* 105 (1996) 3883.
- [14] J.D. McNeill, R.L. Lingle, Jr., N.-H. Ge, C.M. Wong, R.E. Jordan, C.B. Harris, *Phys. Rev. Lett.* 79 (1997) 4645.
- [15] C.M. Wong, J.D. McNeill, K.J. Gaffney, N.-H. Ge, A.D. Miller, S.H. Liu, C.B. Harris, *J. Phys. Chem. B* 103 (1999) 282.
- [16] W. Berthold, U. Höfer, P. Feulner, D. Menzel, *Chem. Phys.* 251 (2000) 123.
- [17] C.B. Harris, N.-H. Ge, R.L. Lingle, Jr., J.D. McNeill, C.M. Wong, *Ann. Rev. Phys. Chem.* 48 (1997) 711.
- [18] P.M. Echenique, J.B. Pendry, *J. Phys. C: Solid State Phys.* 11 (1978) 2065.
- [19] R.W. Schoenlein, J.G. Fujimoto, G.L. Eesley, T.W. Capehart, *Phys. Rev. B* 43 (1991) 4688.
- [20] U. Höfer, I.L. Shumay, Ch. Reuß, U. Thomann, W. Wallauer, Th. Fauster, *Science* 277 (1997) 1480.
- [21] M. Weinelt, *J. Phys.: Condens. Matter* 14 (2002) R1099.
- [22] R. Haight, *Surf. Sci. Rep.* 21 (1995) 275.
- [23] P.M. Echenique, J.B. Pendry, *Prog. Surf. Sci.* 32 (1989) 111.
- [24] N.V. Smith, *Phys. Rev. B* 32 (1985) 3549.
- [25] B. Reihl, K.H. Frank, R.R. Schlittler, *Phys. Rev. B* 30 (1984) 7328.
- [26] B. Reihl, *Surf. Sci.* 162 (1985) 1.
- [27] D.F. Padowitz, W.R. Merry, R.E. Jordan, C.B. Harris, *Phys. Rev. Lett.* 69 (1992) 3583.
- [28] W.R. Merry, R.E. Jordan, D.F. Padowitz, C.B. Harris, *Surf. Sci.* 295 (1993) 393.
- [29] M. Wolf, E. Knoesel, T. Hertel, *Phys. Rev. B* 54 (1996) 5295.
- [30] W. Berthold, F. Rebenrost, P. Feulner, U. Höfer, *Appl. Phys. A* 78 (2003).
- [31] M.W. Cole, M.H. Cohen, *Phys. Rev. Lett.* 23 (1969) 1238.
- [32] M.W. Cole, *Phys. Rev. B* 3 (1971) 4418.
- [33] P.M. Echenique, F. Flores, F. Sols, *Phys. Rev. Lett.* 55 (1985) 2348.
- [34] P. de Andres, P.M. Echenique, F. Flores, *Phys. Rev. B* 35 (1987) 4529; P.L. de Andres, P.M. Echenique, F. Flores, *Phys. Rev. B* 39 (1989) 10356.
- [35] S. Gao, B.I. Lundqvist, *Prog. Theor. Phys. Suppl.* 106 (1991) 405.
- [36] S. Gao, B.I. Lundqvist, *Solid State Commun.* 84 (1992) 147.
- [37] E.V. Chulkov, V.M. Silkin, P.M. Echenique, *Surf. Sci.* 437 (1999) 330.
- [38] E.V. Chulkov, V.M. Silkin, P.M. Echenique, *Surf. Sci.* 391 (1997) L1217.
- [39] E.V. Chulkov, I. Sarria, V.M. Silkin, J.M. Pitarke, P.M. Echenique, *Phys. Rev. Lett.* 80 (1998) 4947.
- [40] J. Kliewer, R. Berndt, E.V. Chulkov, V.M. Silkin, P.M. Echenique, S. Crampin, *Science* 288 (2000) 1399.

- [41] W. Berthold, U. Höfer, P. Feulner, E.V. Chulkov, V.M. Silkin, P.M. Echenique, *Phys. Rev. Lett.* 88 (2002) 056805.
- [42] I. Sarria, J. Osma, E.V. Chulkov, J.M. Pitarke, P.M. Echenique, *Phys. Rev. B* 60 (1999) 11795.
- [43] Th. Fauster, W. Steinmann, in: P. Halevi (Ed.), *Electromagnetic Waves: Recent Developments in Research*, North-Holland, Amsterdam, 1995, p. 350.
- [44] A.G. Borisov, A.K. Kazansky, J.P. Gauyacq, *Phys. Rev. B* 59 (1999) 10935.
- [45] A.G. Borisov, A.K. Kazansky, J.P. Gauyacq, *Phys. Rev. B* 65 (2002) 205414.
- [46] P.M. Echenique, J. Osma, M. Machado, V.M. Silkin, E.V. Chulkov, J.M. Pitarke, *Prog. Surf. Sci.* 67 (2001) 271.
- [47] E.V. Chulkov, V.M. Silkin, M. Machado, *Surf. Sci.* 482–485 (2001) 693.
- [48] M. Machado, W. Berthold, E.V. Chulkov, U. Höfer, P.M. Echenique, *Phys. Rev. B*, to be published.
- [49] P.M. Echenique, J.M. Pitarke, E.V. Chulkov, A. Rubio, *Chem. Phys.* 251 (2000) 1.
- [50] L. Hedin, S. Lundqvist, *Solid State Phys.* 23 (1969) 1.
- [51] U. von Barth, B. Holm, *Phys. Rev. B* 54 (1996) 8411.
- [52] B. Holm, U. von Barth, *Phys. Rev. B* 57 (1998) 2108.
- [53] J. Lindhard, K. Dan, *Vidensk. Selsk. Mat.-Fys. Medd.* 28 (8) (1954).
- [54] A. Eguiluz, *Phys. Rev. B* 31 (1985) 3303.
- [55] V.M. Silkin et al., in press.
- [56] G. Perluzzo, G. Bader, L.G. Caron, L. Sanche, *Phys. Rev. Lett.* 55 (1985) 545.
- [57] N. Schwentner, E.-E. Koch, J. Jortner, *Electronic Excitations in Condensed Rare Gases*, Springer-Verlag, Berlin, 1985.